Cell Stem Cell, Volume *20*

Supplemental Information

Adipocyte Accumulation in the Bone Marrow during Obesity and Aging Impairs Stem Cell-Based Hematopoietic and Bone Regeneration

Thomas H. Ambrosi, Antonio Scialdone, Antonia Graja, Sabrina Gohlke, Anne-Marie Jank, Carla Bocian, Lena Woelk, Hua Fan, Darren W. Logan, Annette Schürmann, Luis R. Saraiva, and Tim J. Schulz

Supplemental Figure 1

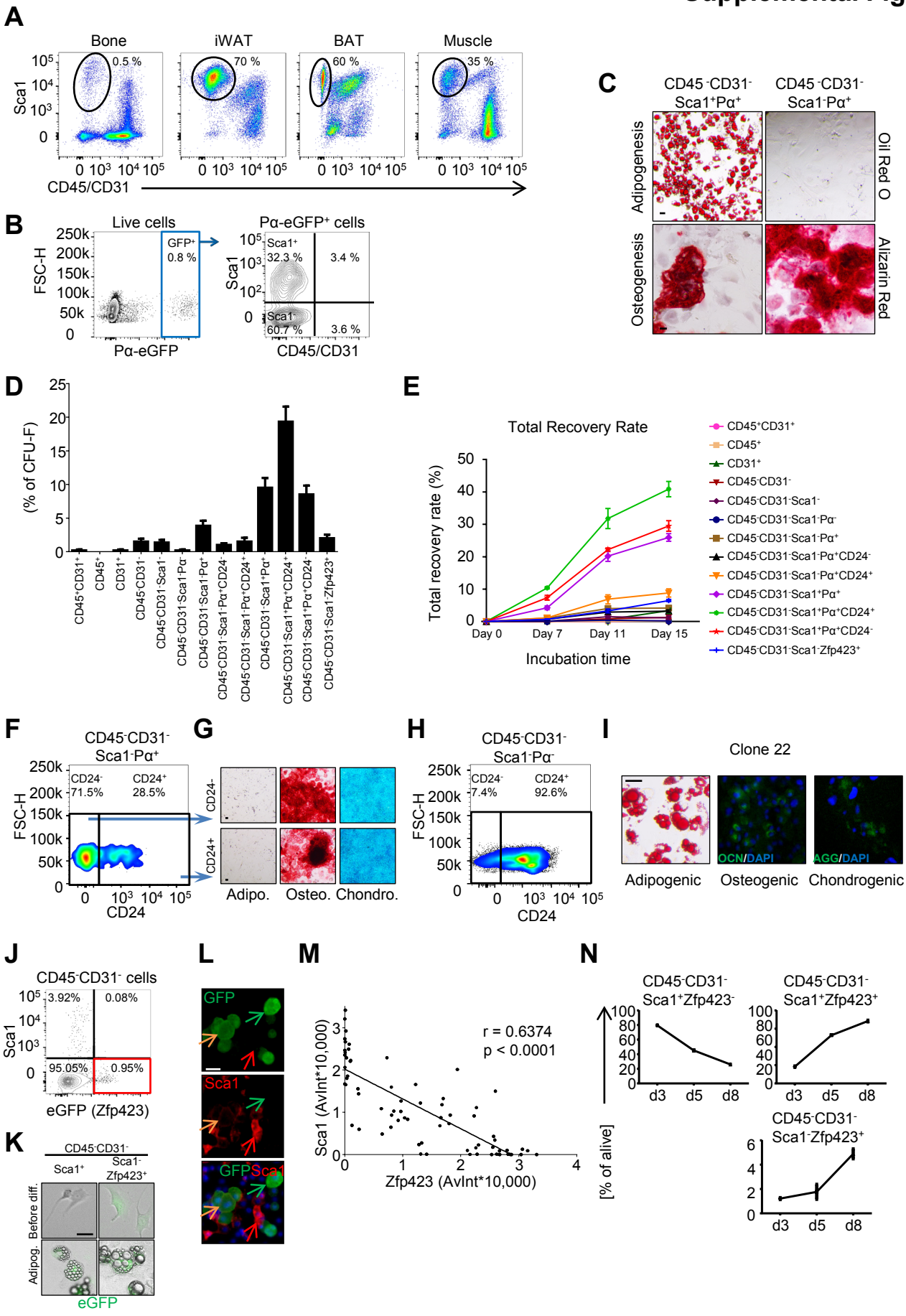

Supplemental Figure 2

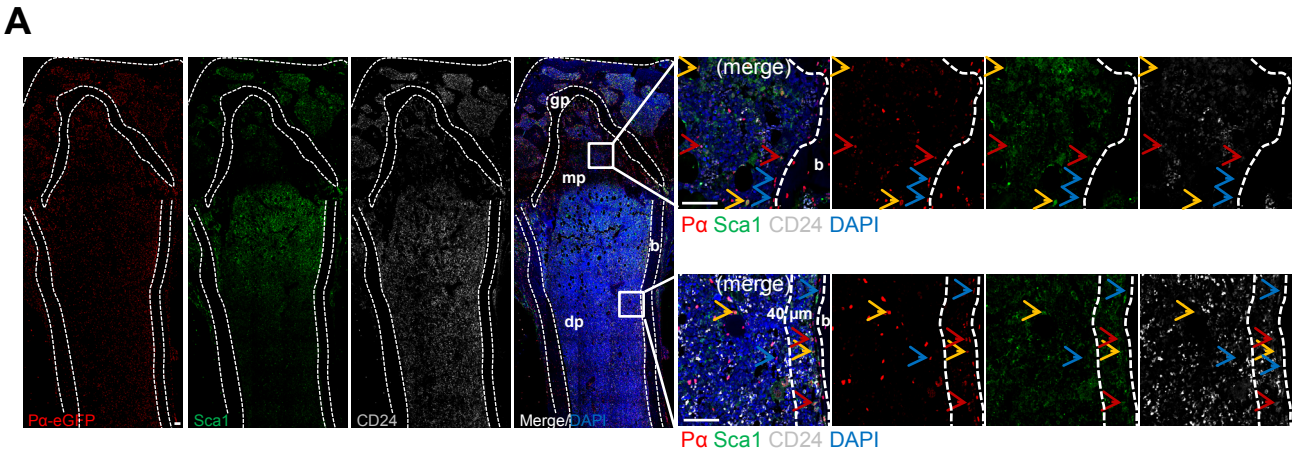

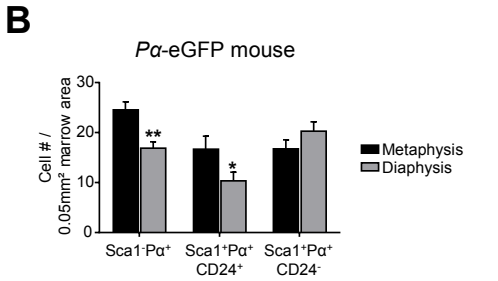

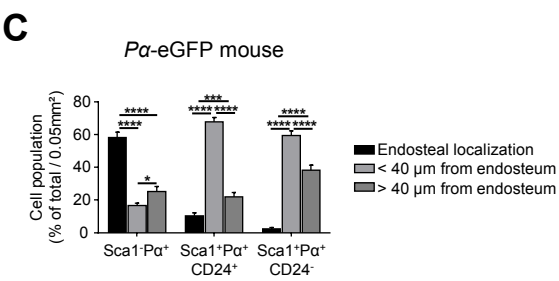

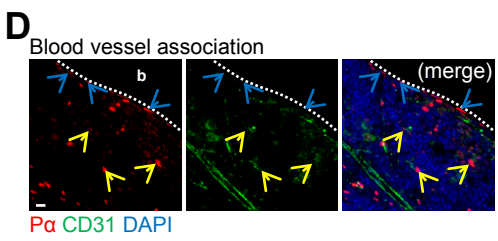

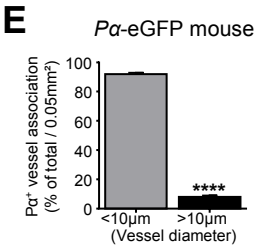

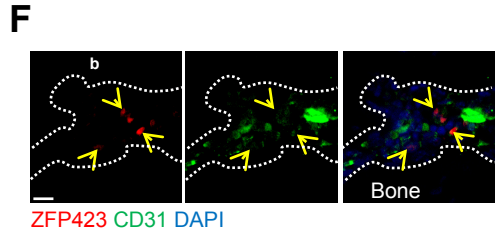

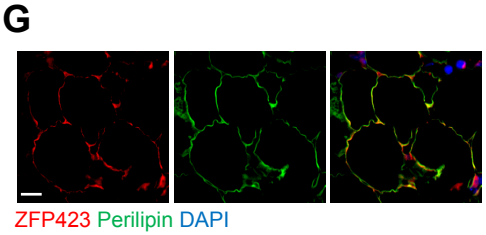

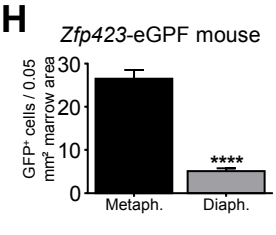

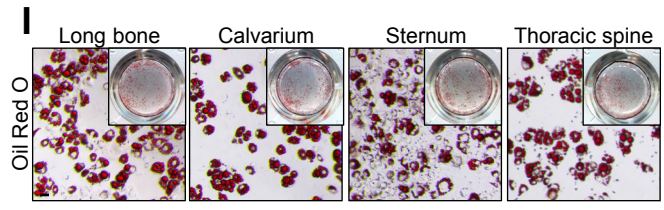

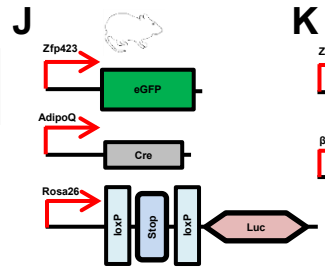

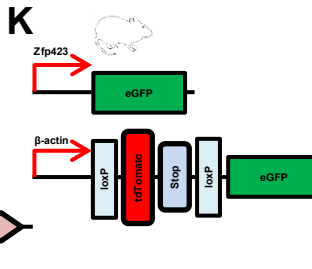

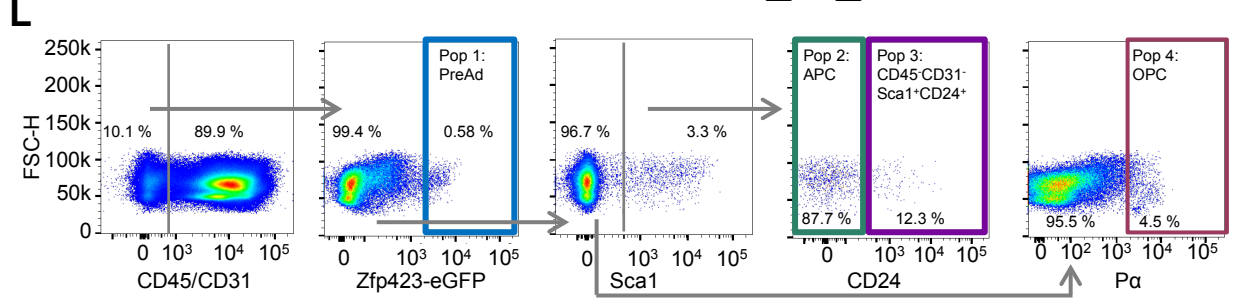

Supplemental Figure 3

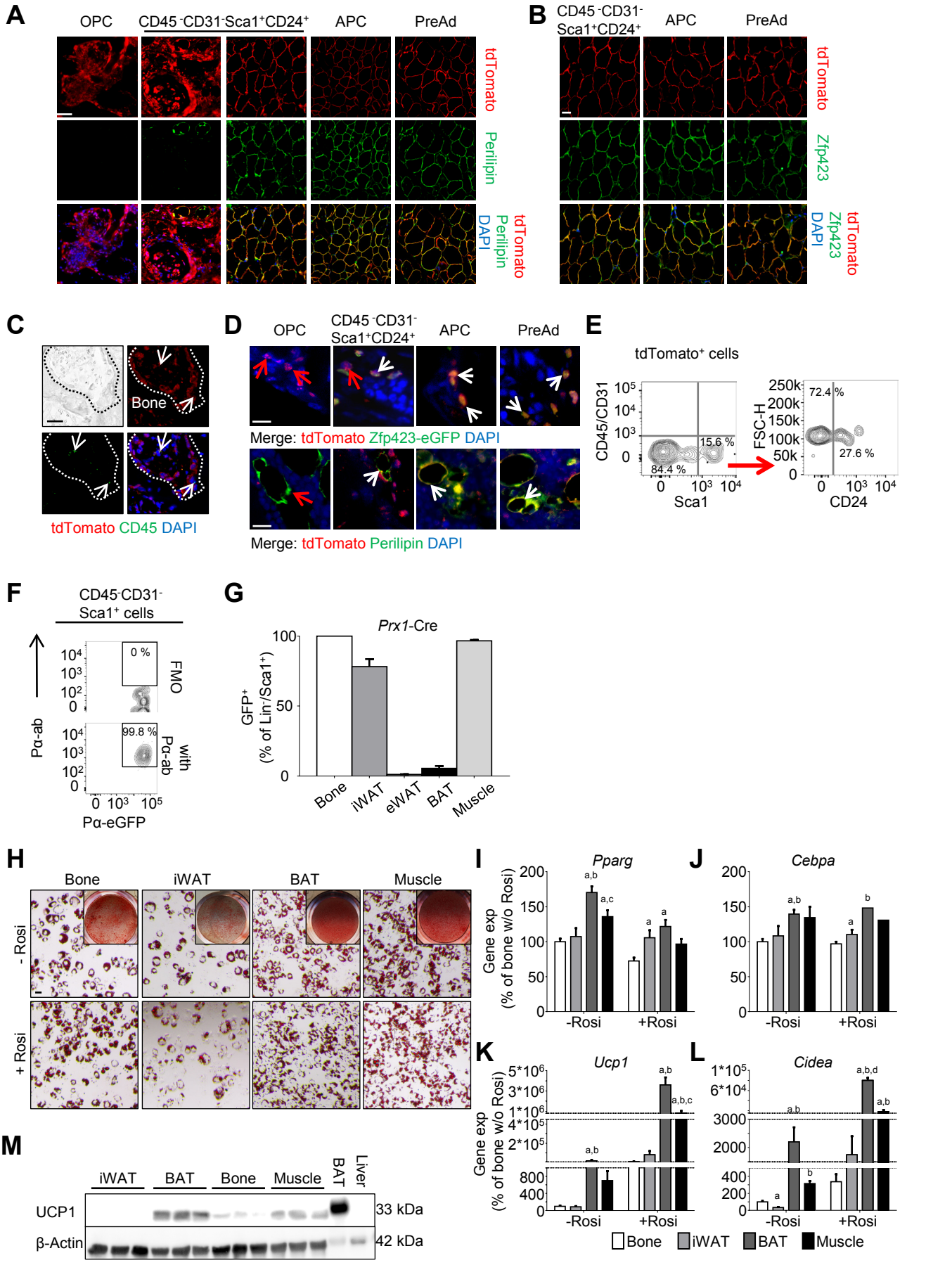

Supplemental Figure 4

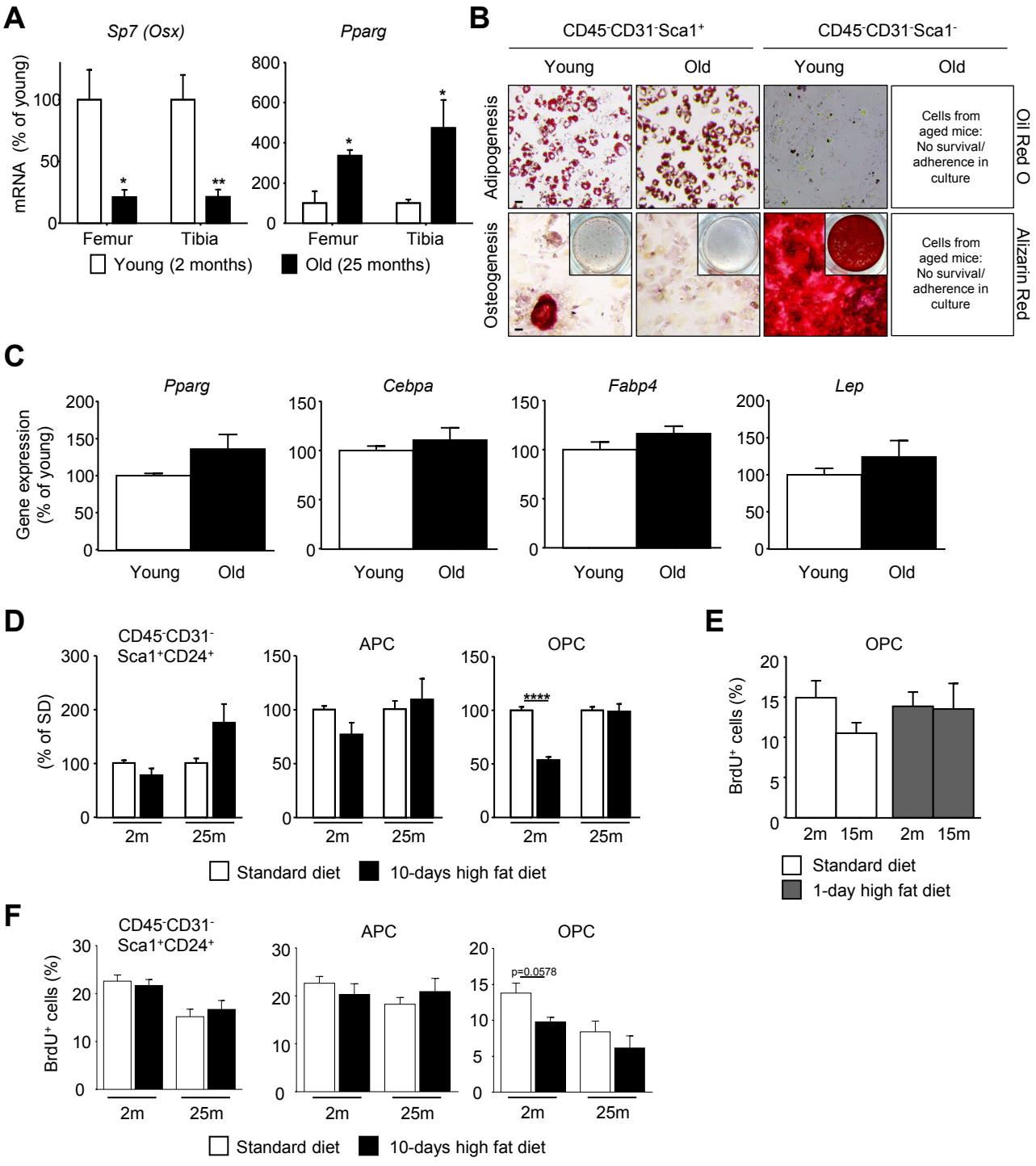

Supplemental Figure 5

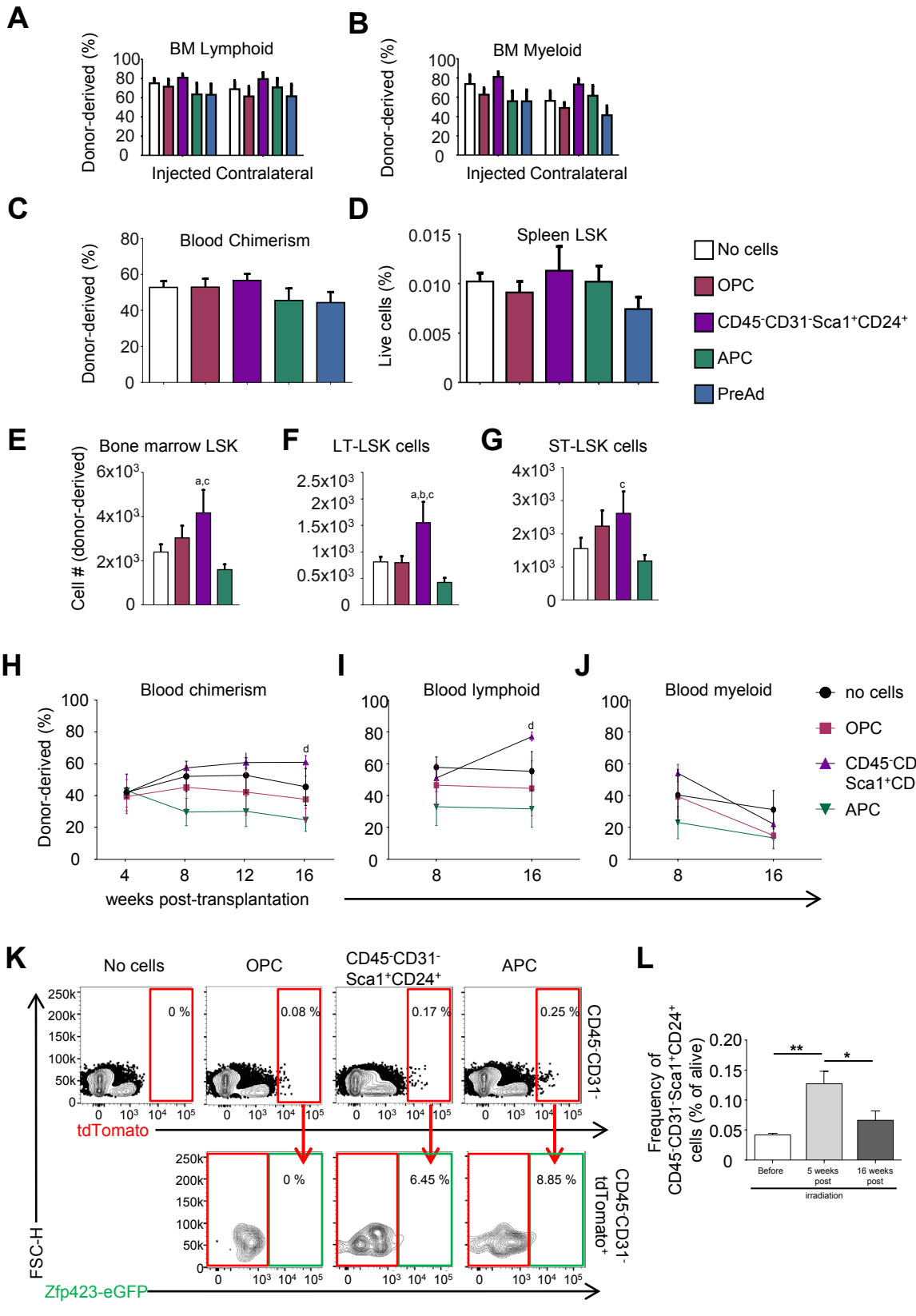

Supplemental Figure 6

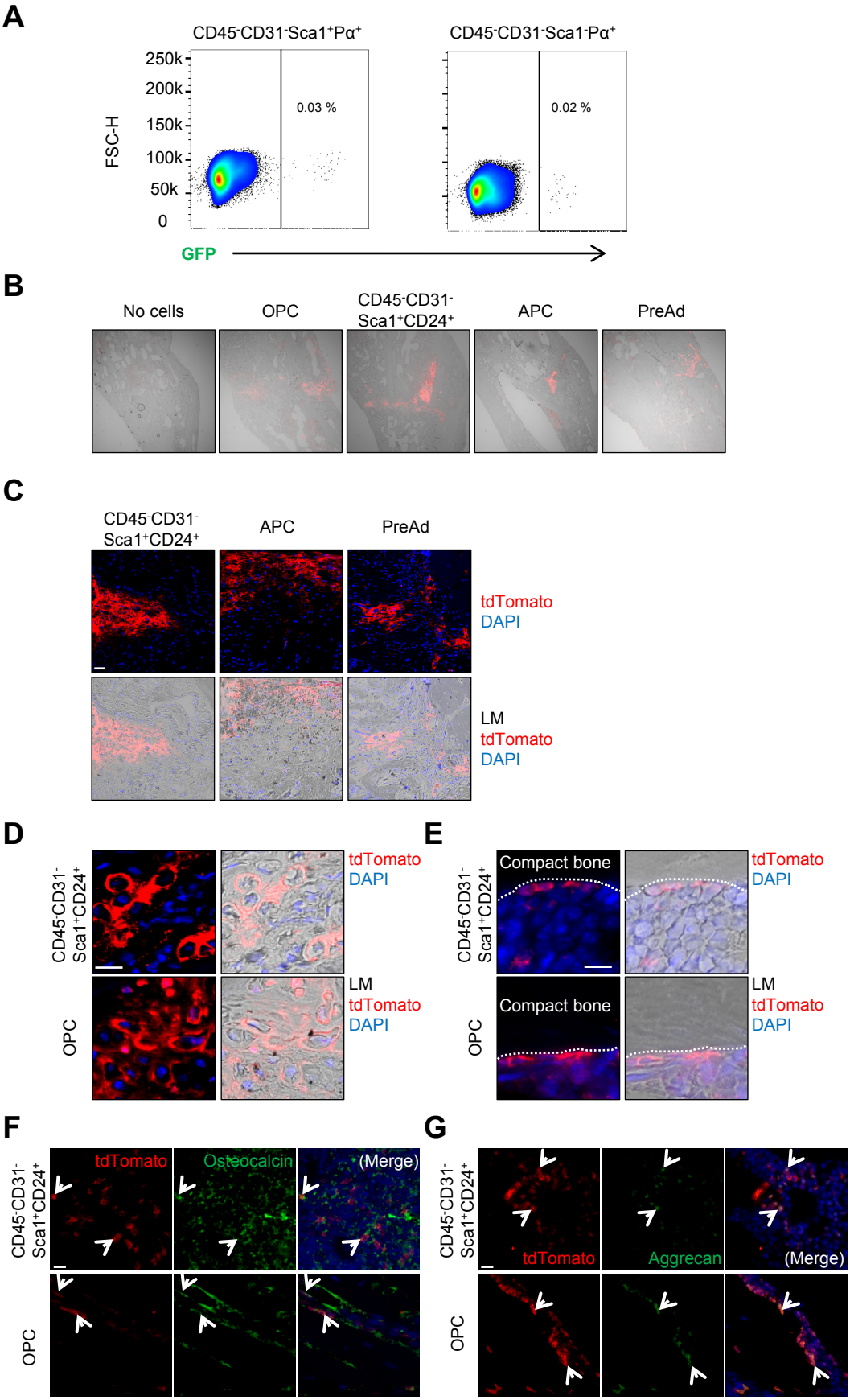

Supplemental Figure 7

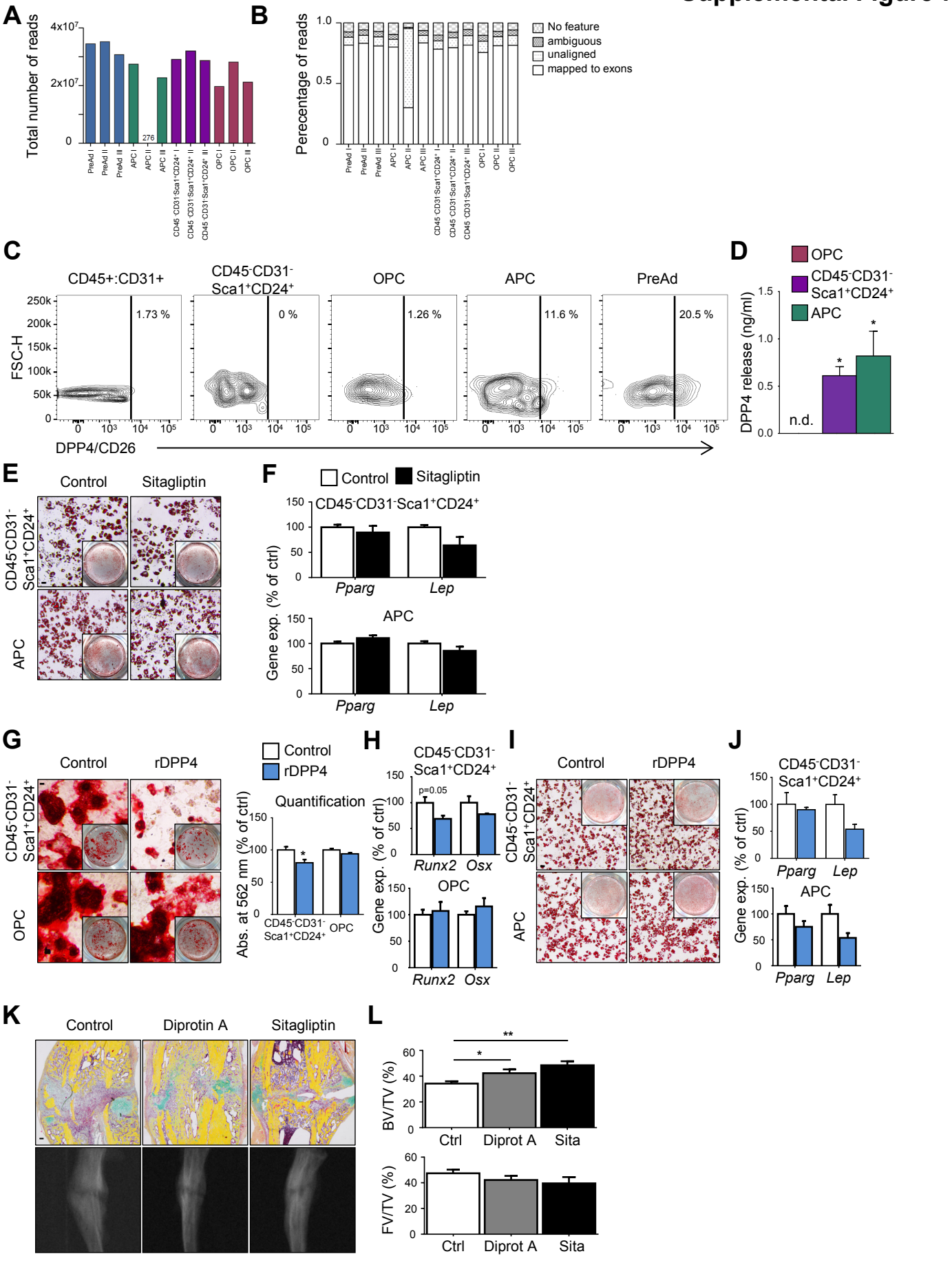

Supplemental Table 1

Differentiation potential	Single-cell co-culture assay (with feeders) # of clones	Single-cell assay (without feeders) # of clones
Adipogenic/ Osteogenic/ Chondrogenic	64 (94.12%)	45 (83.33%)
Adipogenic/ Osteogenic	2 (2.94%)	1 (1.85%)
Adipogenic/ Chondrogenic	1 (1.47%)	-
Osteogenic/ Chondrogenic	-	-
Adipogenic only	1 (1.47%)	4 (7.42%)
Osteogenic only	-	3 (5.55%)
Chondrogenic only	-	
none	-	1 (1.85%)
Total # of clones	68	54

Supplemental table 2

Population (% of viable cells)	Long bones	Sternum	Thoracic vertebra	Caudal vertebra	Calvarium
Multi-potent stem cell ($CD45^-CD31^-Sca1^+CD24^+$)	$0.03967^{c} \pm 0.0043$	$0.032^{c} \pm 0.003$	0.23 ± 0.065	$0.03967^{c} \pm 0.006$	$0.04767^{c} \pm 0.004$
Osteochondrogenic progenitor cell (OPC)	$0.51^{c,d,e} \pm 0.038$	$0.47^{c,d,e} \pm 0.01$	$1.077^{d,e} \pm 0.23$	$0.6133^{e} \pm 0.024$	0.78 ± 0.023
Adipogenic progenitor cell (APC)	$0.18^{c} \pm 0.015$	$0.07333^{c} \pm 0.023$	0.6267 ± 0.08	$0.1467^{c} \pm 0.007$	$0.109^{c} \pm 0.007$
Pre-adipocyte (preAd)	$0.1333^{b,c,d,e} \pm 0.033$	$0.09133^{c,d} \pm 0.019$	$0.02567^{e} \pm 0.003$	0.04733 ± 0.01	0.07333 ± 0.003

Supplemental Table 3

Transplant fate \ Cell population	OPC	CD45$^-$CD31$^-$Sca1$^+$CD24$^+$	APC	preAd
Adipogenic	-	2	13	5
Osteochondrogenic	9	2	-	-
Adipog. & osteochondr.	-	3	-	-
No engraftment	2	3	3	1
n (animals)	11	10	16	6

Supplemental table 4

Population	Immunophenotypes/ Marker phenotypes	Adipogenic potential	Osteogenic potential	Chondrogenic potential
Multi-potent stem cell-like population	**CD45$^-$CD31$^-$Sca1$^+$**Pα$^+$**CD24$^+$** Zfp423$^-$	*In vitro,* sternal transplant, fracture model, irradiation model	*In vitro*, sternal transplant, fracture model	*In vitro*, sternal transplant, fracture model
Osteochondrogenic progenitor cell (**OPC**)	**CD45$^-$CD31$^-$ Sca1$^-$Pα$^+$**CD24$^{+/-}$Zfp423$^-$	**No adipogenesis**	*In vitro*, sternal transplant, fracture model	*In vitro*, sternal transplant, fracture model
Adipogenic progenitor cell (**APC**)	**CD45$^-$CD31$^-$ Sca1$^+$**Pα$^+$**CD24$^-$** Zfp423$^-$	*In vitro*, sternal transplant, fracture model, irradiation model	**No osteogenesis**	**No chondrogenesis**
Pre-adipocyte (**preAd**)	**CD45$^-$CD31$^-$Sca1$^-$** CD24$^-$**Zfp423$^+$**	*In vitro*, sternal transplant, fracture model, irradiation model	**No osteogenesis**	**No chondrogenesis**

Supplemental table 6

Gene	Sequence (5'→3')	Species	Accession No.
Cebpa	Fwd: AGTCGGTGGACAAGAACAGC Rev: TCACTGGTCAACTCCAGCA	mouse	NM_007678
Cidea	Fwd: ATCACAACTGGCCTGGTTACG Rev: TACTACCCGGTGTCCATTTCT	mouse	NM_007702
Dpp4	Fwd: CGGTATCATTTAGTAAAGAGGCAAA Rev: GTAGAGTGTAGAGGGGCAGACC	mouse	NM_010074
Fabp4	Fwd: GATGCCTTTGTGGGAACCT Rev: CTGTCGTCTGCGGTGATTT	mouse	NM_024406
Lep	Fwd: CCTCATCAAGACCATTGTCACC Rev: TCTCCAGGTCATTGGCTATCTG	mouse	NM_008493
Ppia	Fwd: CAAATGCTGGACCAAACACAA Rev: AAGACCACATGCTTGCCAT	mouse	NM_008907
Pparg	Fwd: CTCCAAGAATACCAAAGTGCGA Rev: GCCTGATGCTTTATCCCCACA	mouse	NM_011146
Osx/Sp7	Fwd: TCCTCGGTTCTCTCCATCTG Rev: GGACTGGAGCCATAGTGAGC	mouse	NM_130458
Runx2	Fwd: TTCAACGATCTGAGATTTGTGGG Rev: GGATGAGGAATGCGCCCTA	mouse	NM_001146038
Ucp1	Fwd: CAAATCAGCTTTGCCTCACTC Rev: TAAGCCGGCTGAGATCTTGT	mouse	NM_009463

Supplemental Figure legends

Supplemental Figure 1, related to Figure 1. Common Progenitor Cell Markers Identify Functionally Distinct Bone Marrow-resident Populations of Mesenchymal Cells. (A) Representative dot plots showing FACS staining for CD31/CD45 (x-axis) and Sca1 (y-axis) of live stroma cells derived from bone, subcutaneous (inguinal) white adipose tissue (iWAT), brown adipose tissue (BAT), and muscle. $CD45^-CD31^-Sca1^+$ cell populations of each tissue are indicated in black circles. **(B)** FACS-analysis of viable cells from 2-month old male *Pα*-EGFP reporter mice for expression of GFP followed by Sca1 and CD45/CD31 expression analysis within GFP^+ cells. **(C)** Adipogenic (Oil Red O) and osteogenic (Alizarin Red S) differentiation assays of $Sca1^+P\alpha^+$ and $Sca1^-P\alpha^+$ populations. **(D, E)** CFU-F (n=6/cell population, D) and total recovery rate (n=3/cell population, E) assays of the indicated bone populations. **(F, G)** Flow cytometric dot plot analysis (F) and adipogenic (Oil Red O), osteogenic (Alizarin Red S), and chondrogenic (Alcian Blue) differentiation potentials (G) of $CD45^-CD31^-Sca1^-P\alpha^+$ cells separated into $CD24^-$ (upper panels) and $CD24^+$ (lower panels) cell populations. **(H)** Dot plot analysis of the bone resident $CD45^-CD31^-Sca1^-P\alpha^-$ cell population by separation into $CD24^-$ and $CD24^+$ cells by FACS. **(I)** Representative image of clonal analysis of single $CD45^-CD31^-Sca1^+CD24^+$ cells grown without feeder layers by staining of clone 22-derived cells for Oil Red O-accumulation, Osteocalcin or Aggrecan to show adipogenic, osteogenic, and chondrogenic differentiation potentials, respectively. **(J)** FACS-analysis of $CD45^-CD31^-$ cells from 2-months old male *Zfp423*-EGFP reporter mice for expression of Sca1 and GFP. **(K)** GFP-fluorescence was assessed in cultured $CD45^-CD31^-Sca1^+$ (left) and $Zfp423^+$ (right) cells before (top panels) and after (bottom panels) adipogenic differentiation. **(L, M)** Analysis (L) and significant correlation (M) of average fluorescence intensities (AvInt) in individual cells (n=72) after immunofluorescence co-staining for Sca1 (red fluorescence) and *Zfp423*-EGFP (green fluorescence) in the $CD45^-CD31^-Sca1^+$ population at day 5 of adipogenic differentiation (green arrow: Sca1-:Zfp423+; orange arrow: Sca1+:Zfp423+; red arrow: Sca1+:Zfp423-). **(N)** FACS-analysis of cultured $Sca1^+$ cells at day 3 (d3), 5 (d5), and 8 (d8) of adipogenesis showing frequencies of $Sca1^-Zfp423^+$, $Sca1^+Zfp423^+$, and $Sca1^-Zfp423^-$ cell populations (n=3). All values are shown as mean ± SEM. Scale bars, 30μm.

Supplemental Figure 2, related to Figure 1. Distinct Anatomical Localization of Bone-resident Progenitor Cell Populations. (A) To left: IF of a representative distal femur from *Pα*-EGFP reporter mice stained for EGFP (red, due to secondary antibody), Sca1 (green), CD24 (white), and DAPI (blue). To right: Metaphyseal (upper right panels) and diaphyseal (lower right panels) areas were enlarged to indicate micro-anatomical localizations of osteogenic $Sca1^-P\alpha^+$ (blue arrows), multipotent $Sca1^+CD24^+P\alpha^+$ (red arrows), and adipogenic $Sca1^+P\alpha^+CD24^-$ (orange arrows) within the endosteum, <40 μm, or >40 μm from the endosteum (areas indicated by broken white lines: b – bone; gp – growth plate; mp – metaphysis; dp – diaphysis). Scale bars, 50μm. **(B)** Quantification of osteogenic $Sca1^-P\alpha^+$, multipotent $Sca1^+P\alpha^+CD24^+$ and adipogenic $Sca1^+P\alpha^+CD24^-$ cells in metaphysis or diaphysis of bones derived from *Pα*-EGFP mice using images as shown in panel A. **(C)** Quantification osteogenic $Sca1^-P\alpha^+$, multipotent $Sca1^+P\alpha^+CD24^+$ and adipogenic $Sca1^+P\alpha^+CD24^-$ cells localizing at the endosteum, or to areas <40 μm from the endosteum, and to areas >40 μm from the endosteal layer using images as shown in panel A. **(D)** Representative IF images of $P\alpha^+$ cell distribution in *Pα*-EGFP mice. $P\alpha\text{-}GFP^+$ cells (red fluorescence due to secondary antibody) either reside in bone-linings, e.g. the endosteum (blue arrows), or associate to $CD31^+$ (green fluorescence) blood vessels distributed within the bone marrow (yellow arrows). Scale bar, 10μm. **(E)** Quantifications of bone marrow-localized $P\alpha\text{-}GFP^+$ cells associated to blood vessels with diameters, e.g. smaller or larger than 10 μm. **(F, G)** IF analysis of bones from *Zfp423*-EGFP mice: $Zfp423^+$ cells (red fluorescence for GFP protein detection) either co-localizing with CD31 (green fluorescence, F) or Perilipin (green fluorescence, G). Yellow arrows indicate blood vessel associated, undifferentiated $Zfp423^+$ cells while only mature $Zfp423^+$ bone marrow adipocytes co-stain with Perilipin. Scale bars, 10μm. **(H)** Quantification of $Zfp423^+$ preAd distribution in bones from the *Zfp423*-EGFP reporter mouse strain in metaphysis or diaphysis. **(I)** Analysis of adipogenic potential (Oil Red O staining) of $CD45^-CD31^-Sca1^+$ populations isolated from different bone compartments by FACS. Scale bar, 30μm. **(J)** Transgene alleles of the rep^{AdiLuc} reporter mouse strain: The *Zfp423*-EGFP reporter mouse strain was crossed to a strain expressing Cre-recombinase under control of the Adiponectin promoter (*Adipoq*-Cre) and a constitutive Luciferase (Luc)-reporter where the Luc-encoding cDNA is suppressed by a loxP-flanked Stop-signal. Thus, in this reporter strain only mature adipocytes expressing the adipogenic marker Adiponectin undergo Cre-mediated recombination. This leads to the excision of the loxP-flanked stop-cassette, activating the expression of Luciferase that can be detected by *in vivo* imaging techniques (reporter strain is referred to as rep^{AdiLuc} throughout the main text). **(K)** Transgene alleles of the rep^{tdTom} reporter mouse strain: The *Zfp423*-EGFP reporter was crossed to an mTmG-reporter mouse strain without presence of a Cre-transgene. Thus, the cells maintained constitutive red fluorescence and can be detected by immunofluorescence for tdTomato or *in vivo* imaging (reporter strain is referred to as rep^{tdTom} throughout the main text). **(L)** FACS-gating strategy for the isolation of the four investigated bone populations from both reporter mouse strains for subsequent *in vivo* transplantation assays. All results are shown as mean ± SEM (n=14-24 bone marrow sections were analyzed from n=4 mice per reporter strain; *p<0.05, **p<0.01, ***p<0.001, ****p<0.0001).

Supplemental Figure 3, related to Figures 1 and 2. MAT Derives From a Multipotent Population with Stem Cell-like Potential and Resembles WAT rather than a BAT. (A, B) IF of sternal-grown tissues derived from transplanted cell populations of rep^{tdTom} reporter mice (Red: tdTomato; Green: Perilipin (A) or *Zfp423*-EGFP (B); Blue: DAPI). Scale bars, 20µm. **(C)** IF of $CD45^-CD31^-Sca1^-P\alpha^+$ OPC derived tissue (red) with donor-derived bone-like structures containing host-derived CD45-expressing cells (green, white arrows). Scale bar, 20µm. **(D)** IF of tdTomato (red) and *Zfp423*-reporter driven GFP (green, top panels) or Perilipin (green, bottom panels) expression (merged with blue DAPI stain) after intratibial injection of donor cells derived from mTmG (no Cre-expression)-*Zfp423*-EGFP (rep^{tdTom}) double-transgenic mice. Red arrows indicate $tdTomato^+$, e.g. donor-derived, cells, white arrows indicate double-positive cells expressing the *Zfp423*-driven reporter, e.g. cells committed to the adipogenic lineage. Scale bar, 10µm. **(E)** FACS-analysis of transplants of initially $CD45^-CD31^-Sca1^+CD24^+$ cells identified by tdTomato-expression show that these cells give rise to the $CD45^-CD31^-Sca1^+CD24^-$ population within the transplant. **(F)** FACS-analysis of bones derived from *Pα*-EGFP mice showing a full overlap of Pα-antibody and EGFP labeled $CD45^-CD31^-Sca1^+$ cells (FMO: fluorescence-minus-one antibody control). **(G)** FACS-analysis of the $CD45^-CD31^-Sca1^+$ population isolated from bone, iWAT, eWAT, BAT, and muscle of *Prx1*-Cre-mTmG reporter mice (n=3). **(H)** Oil Red O stain of $CD45^-CD31^-Sca1^+$ progenitor cells FACS-isolated from long bone, iWAT, BAT und skeletal muscle with and without exposure to browning agent rosiglitazone (Rosi) during differentiation. Scale bar, 30 µm. **(I-L)** mRNA levels of general adipogenic markers *Pparg* (I) and *Cebpa* (J) as well as brown adipogenic markers *Ucp1* (K) and *Cidea* (L) after adipogenic differentiation (as in C). Results of two independent experiments with 3 replicates each are shown as mean ± SEM (n=6; $p<0.05$: a vs. Bone, b vs. iWAT, c vs. BAT, d vs. Muscle). **(M)** Western blot analysis UCP1 protein and β-Actin as loading control of differentiated $CD45^-CD31^-Sca1^+$ populations after adipogenic differentiation in the presence of Rosi (as in H).

Supplemental Figure 4, related to Figure 3. Aging and High-fat Diet Stimulate Proliferation and Differentiation of Adipogenic Cells While Inhibiting Osteogenic Cells. (A) Gene expression analysis of Sp7 (*Osx*) and *Pparg* in whole-bones (femur and tibia) from young (2 months) and old (25 months) male C57BL/6J mice (n=4). **(B)** Adipogenic (Oil Red O) and osteogenic (Alizarin Red S) differentiation potential of isolated $CD45^-CD31^-Sca1^+$ and $CD45^-CD31^-Sca1^-$ cells derived from young (2 months) and old (25 months) male C57BL/6J mice. Scale bars, 30 µm. **(C)** Gene expression analyses of *Pparg*, Cebpa, *Fabp4* and *Leptin* (*Lep*) in young and old $Sca1^+$ cells after adipogenic differentiation. Results are shown as mean ± SEM of two independent experiments (n=6). **(D)** Quantification of multipotent $CD45^-CD31^-Sca1^+CD24^+$, adipogenic $CD45^-CD31^-Sca1^+CD24^-$ (APC), and osteogenic $CD45^-CD31^-Sca1^-P\alpha^+$ (OPC) subpopulations in young (2 months) and old (25 months) male mice fed SD or high fat diet for 10 days (10dHFD) (n=9). **(E)** Quantification of BrdU incorporation into bone-resident $CD45^-CD31^-Sca1^-P\alpha^+$ cells in young (2 months) and old (15 months) mice after 1dHFD compared to mice fed a SD (n=7-8). All graphs show cumulative data from at least three independent experiments. **(F)** Quantification of BrdU incorporation into multipotent $CD45^-CD31^-Sca1^+CD24^+$, adipogenic $CD45^-CD31^-Sca1^+CD24^-$ (APC), and osteogenic $CD45^-CD31^-Sca1^-P\alpha^+$ (OPC) subpopulations in young (2 months) and old (25 months) mice after 10dHFD compared to mice fed a SD (n=3). All results are shown as mean ± SEM (*$p<0.05$; **$p<0.01$).

Supplemental Figure 5, related to Figure 4. Level of Adipogenic Maturation Determines Functional Role During Hematopoietic Recovery. (A, B) Donor-derived bone marrow (BM) lymphoid (A) and myeloid (B) cell populations in BM of injected and contralateral tibiae of irradiated mice 5 weeks after irradiation/transplantation. **(C)** Blood chimerism and (**D**) splenic LSKs 5 weeks post transplantation**. (E)** Donor-derived LSK, (**F**) LT-LSK, and (**G**) ST-LSK hematopoietic stem cells in injected tibiae 16 weeks after irradiation/transplantation. $p<0.05$: a vs. no cells; b vs. $CD45^-CD31^-Sca1^-P\alpha^+$; c vs. $CD45^-CD31^-Sca1^+CD24^-$ **(H)** Blood chimerism showing donor-derived blood cells at 4, 8, 12, and 16 weeks post transplantation. **(I)** Donor-derived bone marrow (BM) lymphoid and (**J**) myeloid cell populations in blood of irradiated mice 8 and 16 weeks after irradiation/transplantation. **(K)** FACS analysis of tibiae to identify transplanted cells from rep^{tdTom} double-transgenic mice 16 weeks after irradiation/transplantation: $CD45^-CD31^-tdTomato^+$ cells (red squares, top row) were gated for expression of GFP (green squares: *Zfp423*-EGFP reporter; bottom row), indicating that transplanted cells show long-term presence. **(L)** The effect of irradiation (7.5 Gy) on the tibia-resident $CD45^-CD31^-Sca1^+CD24^+$ cell population. All results are displayed as mean ± SEM (n=4-8; *$p<0.05$, **$p<0.01$).

Supplemental Figure 6, related to Figure 5. The Adipocytic Lineage Inhibits Bone Healing. (A) Flow cytometric analysis of fracture calluses two weeks after surgery either injected with bone-derived $Sca1^+P\alpha^+$ cells or $Sca1^-P\alpha^+$cells isolated from animals constitutively expressing GFP. Shown are viable cells previously gated for $CD45^-CD31^-$ to show retention of cells after transplantation. **(B)** Merged images of IF analysis of tdTomato expression and light microscopy of fracture calluses injected with tdTomato-labelled cells (red fluorescence) of the indicated population. **(C)** IF of fracture site showing fibrous tissue areas derived from injected tdTomato-labelled

(red) in the multipotent CD45$^-$CD31$^-$Sca1$^+$CD24$^+$, adipogenic CD45$^-$CD31$^-$Sca1$^+$CD24$^-$ (APCs), and CD45$^-$CD31$^-$Sca1$^-$Zfp423$^+$ (preAd) subpopulations that were not observed in transplants from osteogenic CD45$^-$CD31$^-$Sca1$^-$Pα$^+$ cells. Scale bars indicate 20 μm. **(D)** IF showing the contribution of transplanted multipotent CD45$^-$CD31$^-$Sca1$^+$CD24$^+$ (upper panels) and osteogenic CD45$^-$CD31$^-$Sca1$^-$Pα$^+$ (OPC, lower panels) cell populations to osteochondrogenic structures in the fractured tibiae that were not observed in adipogenic cell transplants (Red: tdTomato; Blue: DAPI; right panels indicate merge of IF and light microscopic images). Scale bar, 20 μm. **(E)** IF showing the contribution of transplanted multipotent CD45$^-$CD31$^-$Sca1$^+$CD24$^+$ (upper panels) and osteogenic CD45$^-$CD31$^-$Sca1$^-$Pα$^+$ (OPC, lower panels) cell populations to endosteal bone linings in the fractured tibiae (Red: tdTomato; Blue: DAPI; dotted lines indicate areas of compact bone as seen in right-side panels of merged IF and light microscopic images). Scale bar, 10 μm. (**F, G**) IF co-staining of tdTomato+ cells (red fluorescence) with Osteocalcin (F) or Aggrecan (G) to show osteogenic and chondrogenic differentiation fates of transplanted multipotent CD45$^-$CD31$^-$Sca1$^+$CD24$^+$ (upper panels) osteogenic CD45$^-$CD31$^-$Sca1$^-$Pα$^+$ (lower panels) cell populations. No co-staining detected in adipogenesis-committed populations, e.g. APCs and preAds (not shown). Scale bar, 10 μm.

Supplemental Figure 7, related to Figures 6 and 7. Delayed Fracture Healing Through Adipogenic Cells is Reversed by DPP4 Inhibition. (A) Results of RNA-Seq samples regarding read counts and (**B**) fraction of reads mapped to exons are displayed. **(C)** FACS analysis of DPP4/CD26 surface marker expression in CD45$^+$CD31$^+$ populations and CD45$^-$CD31$^-$Sca1$^+$CD24$^+$, CD45$^-$CD31$^-$Sca1$^-$Pα$^+$ (OPC), CD45$^-$CD31$^-$Sca1$^+$CD24$^-$ (APC) and CD45$^-$CD31$^-$Sca1$^-$Zfp423$^+$ (preAd) populations of 2-months old male mice. **(D)** DPP4 release into the culture medium by OPCs, multipotent CD45$^-$CD31$^-$Sca1$^+$CD24$^+$, and CD45$^-$CD31$^-$Sca1$^+$CD24$^-$ cell populations that underwent *in vitro* adipogenic differentiation (n=3). **(E)** Oil Red O staining and (**F**) mRNA expression levels of *Pparg* and *Lep* in multipotent CD45$^-$CD31$^-$Sca1$^+$CD24$^+$ and APCs (CD45$^-$CD31$^-$Sca1$^+$CD24$^-$) either treated with PBS (control; white bars) or Sitagliptin (100 μM, black bars) during adipogenic differentiation (n=6 from two independent experiments). **(G)** Alizarin Red S staining and quantification, and (**H**) mRNA expression levels of *Osx* and *Runx2* in multipotent CD45$^-$CD31$^-$Sca1$^+$CD24$^+$ and OPCs (CD45$^-$CD31$^-$Sca1$^-$Pα$^+$) either treated with PBS (control; white bars) or recombinant mouse rDPP4 (250 ng/mL; blue bars) during osteogenic differentiation (n=3). **(I)** Oil Red O staining and (**J**) mRNA expression levels of *Pparg* and *Lep* in multipotent CD45$^-$CD31$^-$Sca1$^+$CD24$^+$ and APCs (CD45$^-$CD31$^-$Sca1$^+$CD24$^-$) cells either treated with PBS (control; white bars) or rDPP4 (250 ng/mL; blue bars) during adipogenic differentiation (n=3). **(K)** Histomorphometric (top panels) analysis and corresponding μCT images (bottom panels) of the fracture callus and (**L**) quantification of mineralized (BV/TV) and fibrotic areas (FV/TV) of mice either treated with PBS, Diprotin A, or Sitagliptin for 9 days (n=6-7). Results are shown as mean ± SEM (*p<0.05; **p<0.01). Scale bars, 30 μm.

Supplemental Table 1, related to Figure 1. Summary of differentiation potential analysis of 68 clones (left column: with feeder layer) and 54 clones (right column: without feeders) derived from single primary CD45$^-$CD31$^-$Sca1$^+$CD24$^+$ cells of bone. See also Figure 1E for a representative image depicting analysis of sample clone 19 from the feeder-based assay and Figure S1F for sample clone 22 of the feeder cell-free clonal assay.

Supplemental Table 2, related to Figure 1. Frequency analyses of the four investigated cell populations in different bone compartments by FACS. All results are displayed as mean ± SEM (n=3; *p<0.05: a vs. long bones; b vs. sternum; c vs. thoracic spine; d vs. caudal spine; e vs. calvarium).

Supplemental Table 3, related to Figure 1. Summary of sternal transplantation experiments of the four investigated cell populations including numbers of transplanted animals and respective differentiation fates as determined by histological analysis and engraftment efficiency with animals were no transplant was found.

Supplemental Table 4. related to Figure 1. Summary of the four investigated cell populations with phenotypic marker expression and differentiation potential performances during *in vitro* and *in vivo* experiments. Column for immunophenotypes/ marker phenotypes: Markers that are required to define and isolate the respective populations by flow cytometry are labeled in bold.

Supplemental Table 5, related to Figure 6. List of genes of RNA-seq displayed in heat maps of Figure 6 as well as expression patterns of genes reported for osteochondrogenic skeletal stem cells (Chan et al., 2015; Worthley et al., 2015).

Supplemental Table 6, related to Figures 7, S3, S4, and S7. Primer sets used in this study.